THEORETICAL AND EXPERIMENTAL INVESTIGATIONS OF TWO-PHASE BUBBLY FLOW THROUGH AN ELECTROCHEMICAL MACHINING GAP

*T.I. Sabry *, N.H. Mahmoud* and A.M. Abdel-Mahboud***

* Department of Mechanical Power Engineering, Faculty of Engineering, Menoufia University, Shebin El-Kom, Egypt.

** Department of Production Engineering and Mechanical Machine Design, Faculty of Engineering, Menoufia University, Shebin El-Kom, Egypt.

ABSTRACT

A theoretical model is proposed in this paper for predicting the distributions of pressure, temperature increasing, mean diameter of bubbles and void fraction within two-phase bubbly flow in an electrochemical machining (ECM) gap. This model is based on equations of mass and energy conservation for unsteady one-dimensional bubbly flow. The experimental program of this work has dealt with using the Phase/Doppler Particle Analyzer (PDPA) technique in two-phase flow measurements through the hydrogen gas layer along the gap. The experiments can release distribution patterns for velocity , size, generation rate and flow rate of hydrogen bubbles besides the thickness of the bubble layer along the tested ECM gap for different applied voltage and electrolyte flow rate.The theoretical results show that the characteristics of the two-phase bubbly flow through an investigated ECM gap were affected by the applied voltage, gap length, electrolyte pressure and electrolyte temperature. Emphasis is placed on a comparison of PDPA measurements for the mean bubbles size and flow void fraction of the bubbles layer with the predictions obtained from the theoretical model. The comparison gives a quite good agreement between the measurements and the present model predictions and also indicates that the one-dimensional flow approximation may be satisfactory for the calculations of the two-phase bubbly flow through a plane ECM gap of rectangular cross-section.

Keywords: Two-phase flow, Void fraction, bubbly flow, Phase Doppler Particle Analyzer, Electrolysis.

INTRODUCTION

Electrochemical machining (ECM) has recently received a considerable attention due to its advantages such as high rate of metal removal, easy to use with complex shaped parts (e.g. turbine and compressor blades), independent toward material properties (e.g. hardness and toughness), no tool wear, etc. [1-5]. In ECM process, metals are dissolved anodically under specific conditions of a small gap between anode and cathode; high current densities and high flow rate of electrolyte through the gap as shown diagramatically in Figure1.

Solutions of NaCl, $NaNO_3$, KCl and KNO_3 are commonly used as electrolytes in ECM process to carry the electric current in the gap, to avoid the formation of insoluble products upon the anode surface and to transmit the heat and hydrogen bubbles from the cathode surface. Hydrogen bubbles may grow from microsizes which were appear primarily upon the solid surface of the cathode until they become large enough to be entrained in the electrolyte stream under the influence of drag forces and surface tension [1,6].

©Faculty of Engineering, Alexandria University-Egypt AEJ 1998

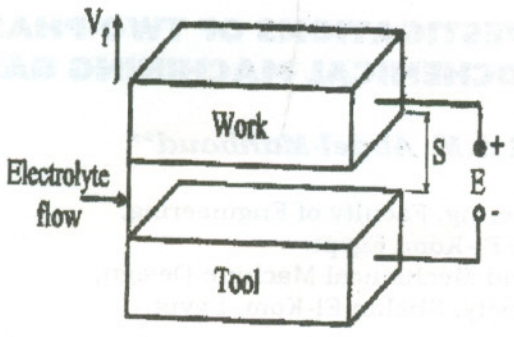

Figure 1 Kinematic Scheme of ECM.

Entrainment of hydrogen bubbles causes it to create a continuous layer (void) at the cathode surface, so that a gas-liquid two-phase flow pattern will occur in the gap. The bubble layer may affect the ECM process due to its high electrical resistance which tends to decrease the current efficiency of metal dissolution process. Therefore, to verify the optimum utilization of ECM process qualitative and quantitative analysis of hydrogen-electrolyte two-phase flow are essentially required.

Modeling of ECM two-phase flow can serve in verifying the effective utilization of ECM process. Several works in the literature [1, 7, 8] have reported numerical models concerning the problems of treating the multiphase flow of ECM process. Most earlier ones of these models use a simplified form of Navier-Stokes equation in one-dimensional or two-dimensional approximations to release a computational procedure for predicting the gap profile [1,9]. On this category of past researches, attention have been devoted to study some parameters such as compressibility effects [7]; pressure distribution [8] and errors of gap shape [10] in ECM processes. The more complex gap geometries which are formed by curved electrodes will have need more advanced models to analyze the two-phase flow through these gaps. Different models concern with analyzing and simulating the two-phase flow through these geometries besides studying the transport phenomena in electrolysers have been presented and discussed by Rousar, *et. al.* [11]. All the reported models were concern only with obtaining the velocity field and pressure variation through the investigated gap. None of the previous models can dedicate an accurate behaviour for the bubbly two-phase flow within an ECM gap.

Evaluating the bubble size and its velocity remains of great importance to understand and explain the hydrodynamics of the two-phase bubbly flow. Numerous techniques for size and velocity measurements of bubbles or drops in gas-liquid or liquid continuum flows were reported in the literature [12]. Optical techniques offer the advantages of; they do not disturb the flow, should be extremely precise, capable of rapid response and are suitable in measurements with high-frequency turbulence fluctuations. Photographic and scattering techniques are mostly used in characterizing the pattern of gas-electrolyte flow along the ECM gap. The high speed photographic technique was used by Landolt, et. al. [13] and Yu, *et. al.* [14] in order to determine the location and size of the bubble layer in an ECM gap. A review for the results of the experimental researches which were used the high speed photographic technique in ECM is presented by McGeough [1]. The photographs which were obtained in some of these investigations [13-14] show the size of individual gas bubbles and its distribution in the gap. These investigations failed in measuring directly either the flow void fraction or the bubble velocity.

Laser techniques offer the nondisturbance advantages of the optical methods while affording a very precise quantitative measurement of velocities. Krishnaiah Chetty and Radhakrishnan [15] used the so called Laser Doppler Velocimeter (LDV) technique for measuring the electrolyte velocity in an experimental ECM setup. Techniques of transmitted and scattered Laser light have been also used by Yu, *et.al.* [14] to measure the void fraction along an ECM gap. The Phase/Doppler method was found to be successful in obtaining a convenient and accurate

measurements for the size and velocity of particle fields. The Phase/Doppler Particle Analyzer (PDPA) technique was used to obtain particle size and velocity measurements for particles of 0.5 to as large as 2000 micrometers [16]. Furthermore, the authors presented a set of flow measurements through an ECM gap with the aid of PDPA technique [17].

Therefore, one of the objectives of the present study is directed towards obtaining a model predicting the distributions of two-phase flow parameters along a plane ECM gap of rectangular cross-section. Whilst the second aims to utilize the PDPA technique for measuring the size and number of hydrogen bubbles as well as their velocity in this gap.

THEORETICAL ANALYSIS

Assumptions

The theoretical model presented below is based on number of assumptions; which in a real system are more or less accurately fulfilled. These assumptions are as follows:

a- The flow is one dimensional and unsteady. The geometry of the model is illustrated in Figure 1.

b- Gas phase consists of monodispersed-spherical hydrogen bubbles with homogeneous distribution across the bubbly fraction in the cross-section of the gap and along the whole electrode surface.

c- Electrolyte or liquid phase is incompressible and with constant properties.

d- Gaseous and liquid phases are assumed to be at the same pressure and velocity.

e- The effect of impurities arising due to material dissolution has been ignored [1,8,11].

f- Heat transfer through electrodes, thermal expansion of the medium and surface heterogeneity from the point of view of electrochemical processes are neglected.

Governing Equations

With the above assumptions and referring to Figure 1, a set of unsteady equations governing the flow and energy transfer in the two phase flow of electrolyte and hydrogen bubbles is presented below.

Generally, mass conservation for one-dimensional unsteady flow is given by

$$\frac{d\rho}{dt}+\frac{d(\rho u)}{dx}=0 \qquad (1)$$

For the continuous medium of electrolyte (liquid) and hydrogen (bubbles) mixture, the equivalent density is defined as

$$\rho=(1-\beta).\rho_e+\beta.\rho_H=\rho_l+\rho_g \qquad (2)$$

Therefore, mass conservation for the electrolyte and the evolved gas are respectively

$$\frac{d\rho_g}{dt}+\frac{d\rho_g u}{dx}=\eta_H.K_H.J \qquad (3)$$

$$\frac{d\rho_l}{dt}+\frac{d\rho_l u}{dx}=\eta_M.K_M.J=-\eta_H.K_H.J \qquad (4)$$

where η_H, K_H, η_M and K_M are current efficiency of hydrogen generation, electrochemical equivalent of hydrogen generation, current efficiency of metal removal and electrochemical equivalent of metal removal respectively. It should be said here that these parameters (i.e., η_H, K_H, η_M and K_M) were selected in the present study for mild steel machined in 10% aqueous solution of NaCl from [1, 5].

Substituting Equation 2 into Equations 3 and 4 and rearranging then results in

$$\frac{d\beta}{dt}+u.\frac{d\beta}{dx}=\frac{1}{\rho_H}.\eta_H.K_H.J \qquad (5)$$

$$\frac{d\alpha}{dt}+u.\frac{d\alpha}{dx}=-\frac{1}{\rho_e}.\eta_H.K_H.J=\frac{1}{\rho_e}.\eta_M.K_M.J \qquad (6)$$

where α is the liquid-phase concentration (or wetness fraction) and equals $(1-\beta)$.

In order to solve Equation 5, variation of gas-phase concentration (i.e., void fraction)

along the gap length is obtained by Lubkowski, *et.al.* [18] as

$$\frac{d\beta}{dx} = \frac{.\eta_H .K_H .J.R_H .T}{u\,.\,S\,.\,P} \qquad (7)$$

where R_H is the gas constant of hydrogen.
It follows that the energy conservation is given by

$$\frac{d}{dt}\left[S.(1-\beta).\rho_e.C_{p_e}.T\right]+\frac{d}{dx}\left[u.S.(1-\beta).\rho_e.C_{p_e}.T\right]=J.E \qquad (8)$$

In Equation 8, J.E represents the electric heat generated in the electrolyte due to current passing through the gap whilst {S. (1-β).ρ_e. C_{pe} .T} denotes the heat imposed in the electrolyte. Carrying out the differentiations indicated in Equation 8. leads to

$$\frac{1}{T}.\frac{dT}{dt}-\frac{1}{1-\beta}.\frac{d\beta}{dt}+\frac{1}{S}.\frac{dS}{dt}+\frac{u}{T}.\frac{dT}{dx}-\frac{u}{1-\beta}.\frac{d\beta}{dx}+\frac{u}{S}.\frac{dS}{dx} = \frac{J.E}{S.(1-\beta).\rho_e.C_{p_e}.T} \qquad (9)$$

Model Formulation

In order to solve Equation 9, the derivatives (dT/dx), (dβ/dx) and (dS/dx) are required at least to be defined for this sake. Firstly, the rate at which the gap between the work piece and the tool changes with feed motion is given by McGeough [1] as;

$$\frac{dS}{dt} = \frac{K_M .\lambda_e .E}{\rho_a .S} - V_f \qquad (10\text{-a})$$

where ρ_a is the density of anode metal.
This rate is changed with zero feed operation to

$$\frac{dS}{dt} = \frac{K_M .\lambda_e .E}{\rho_a .S} \qquad (10\text{-b})$$

Thus, an expression for electrolyte temperature variation along the gap (dT/dx) is derived starting from Ohm's law to obtain the following relationship for the average current density across the gap

$$J = \frac{I}{a} = \frac{\lambda_e .E}{S} \qquad (11)$$

This average current density creats heat in a length dx of the gap equals (J^2.dx). Using Joule's and Ohm's laws and considering that all the heat caused by the current transmitting can be transferred to the electrolyte yields to

$$J^2.dx = \lambda_e .\rho_e .C_{p_e} .u.dT \qquad (12)$$

Rearranging Equation 12 gives

$$\frac{dT}{dx} = \frac{J^2}{\lambda_e .\rho_e .C_{p_e} .u} \qquad (13)$$

Now, Equation 9 can be solved using Equations 7, 10-a or 10-b and 13.
Derivation of mean bubble size variation along the gap is obtained here using a definition for the void fraction of a bubbly gas-liquid mixture as ;

$$\beta = \frac{V_g}{V_g + V_l} \qquad (14)$$

Volume of mixture element occupied by the gaseous fraction in Equation 14 is given for spherical bubbles by

$$V_g = N.\frac{4}{3}\pi r^3 \qquad (15)$$

Introducing Equation 15 into Equation 14, one obtains the following

$$N.\frac{4}{3}\pi r^3 = V_l .\frac{\beta}{1-\beta} \qquad (16)$$

Differentiation of Equation 16 gives

$$\frac{4}{3}\pi r^3 N.\frac{3}{r}.dr = \frac{1}{(1-\beta)^2}.d\beta \qquad (17)$$

Thus, from Equations 14, 16 and 17, it follows that

$$\frac{dr}{r}=\frac{1}{3}.\frac{1}{1-\beta}.\frac{d\beta}{\beta}$$

or

$$\frac{dr}{dx}=\frac{r}{3}.\frac{1}{\beta(1-\beta)}.\frac{d\beta}{dx} \qquad (18)$$

Then, time variation of mean bubble size can be written as

$$\frac{dr}{dt}=u.\frac{dr}{dx} \qquad (19)$$

Finally, the pressure gradient along the gap is assumed to be given by the following equation which was deduced by Lubkowski *et al.*[18] for similar situations

$$\frac{dP}{dx}=-0.067\frac{\nu^{0.25}.u^{1.75}.(1+A\beta)^{0.25}.\rho_e.e^{B(T-T_o)}}{S^{1.25}} \qquad (20)$$

where A and B are constants and equal 5.5 and -0.019 respectively. Similarly as given by Equation 19, the pressure variation by time is provided by

$$\frac{dP}{dt}=u.\frac{dP}{dx} \qquad (21)$$

Besides the above basic equations, a set of supplementary equations is released below to complete the suggested model. The first equation gives hydrogen density utilizing equation of state for an ideal gas to obtain

$$\rho_H=\frac{P}{R_H.T} \qquad (22)$$

The second equation evaluates the conductivity of the two-phase mixture, in the whole β range of ECM, due to [1] as

$$\lambda=\lambda_e.(1+\varepsilon.\Delta T).(1-\beta)^{1.5} \qquad (23)$$

where ε is the temperature coefficient of conductivity which can be taken approximately equals to 0.02 for salt solutions [5].

The next one is utilized by Lubkowski, *et. al.* [18] to calculate the absolute viscosity of the two-phase mixture as a function of electrolyte absolute viscosity (μ_e) by

$$\mu=\mu_e.(1+A\beta).e^{B(T-T_i)} \qquad (24)$$

where T_i is the initial flow temperature. Constants A and B in Equation 24, were defined above with Equation 20.

The last equation deals with obtaining the bubbles departure size. The following expression for this size was derived on the basis of the author's own investigations and literature [19,20]. This expression utilizes the theory of capillarity to get an equilibrium bubble shape under the balance of gravity and surface tension forces and namely as

$$d_{o_i}=4.61\left[\left(\frac{\gamma_e-\gamma_H}{10^3 g}\right)^3\right]^{\frac{1}{2}} \qquad (25)$$

where γ_e and γ_H are the specific weights in N/m^3 of electrolyte and hydrogen respectively and d_{oi} is obtained in mm.

Solution procedure

The system of partial differential Equations 9-21 together with the supplementary algebraic Equations 22-25 provide a set of equations for calculating the bubbly two-phase flow in a rectangular gap. The equations have been solved by means of the general finite-difference procedure of four-point explicit scheme in Reference 11. Approximately 100 iterations, depending on the boundary conditions, were required to perform a satisfactory convergence. The solution procedure is carried out under the following boundary conditions:

At gap entrance (i=1): $P(i) = P_i$, $T(i)=T_i, \beta(i)= 0$
$d(i) = 0$, $\lambda(i) = \lambda e$, $\mu(i) = \mu_e$

At gap exit (i=n) : $P(i) = P_o$

The iterations are repeated until the assumed accuracies are obtained. During solution procedure, the program is stopped at

$T_{max} < T(i)$, $\beta_{max} < \beta(i)$, $u/C > 1$

where C, T_{max} and β_{max} are the local speed of sound, limiting temperature and maximum void fraction which must not be exceeded. More details about the solution procedure (and the flow chart of the computational procedure which was designed and carried out for this procedure) were presented in References 10 and 18. Finally, thermodynamic properties and other physical characteristics which are required in solving the model suggested above are obtained due to [21,22].

EXPERIMENTAL PROGRAM

Experimental setup

Figure 2-a shows a schematic diagram for the experimental ECM setup. It consists of a rectangular flow channel cell of width z = 10 mm and height S = 5 mm, see Figure 2-b . The cathode and the anode of 50 mm length were made of Steel 37 (Carbon: 0.2%). The rectangular flow channel was made using two flat prespex plates enclosing the cathode and the anode and allow the electrolyte to pass into the gap between the opposing faces of the cathode and the anode. Four pieces of wood were used to insulate the cathode and the anode and to extend the flow channel as illustrated in Figure 2-a. The two prespex plates enclose these pieces of wood beside the cathode and the anode in order to provide the transparency along the gap and the flow channel. Furthermore, two rectangular prespex pipes with cross-sectional area of each equals the gap area were used to elongate the flow channel in order to minimize the hydraulic losses along the gap. Sodium chloride solution, 10% by weight, was used as the electrolyte. The electrolyte was pumped using a centrifugal pump of 10 lit/min capacity and at a pressure intensity of 2.5 bar. The electrolyte was supplied from a plastic tank of 100 liter capacity to the cell through the pump and a valve. The electrolyte was allowed to flow in the cell and then returned through a filter to the tank. The electrolyte mass flow rate was measured using a digital balance with sensitivity of 0.1 g and ± 0.02% error and a stop watch to weighing a sample of electrolyte. Another tank filled with fresh water was used to flush the cell after each experiment.

The cathode and the anode were connected to a DC source. The DC source had a maximum output of 600 Amperes and 30 Volts.

The cell was mounted on a table by means of two bolted wooden pieces. This table was supported on a traversing system with two orthogonal motions, one is vertical and the other is horizontal, see Figures 2-a and 2-b.

Measuring Technique

Figure 2-b indicates a general layout for the socalled Phase/Doppler Particle Analyzer (PDPA) technique which was used in the present work to measure the bubbles size and velocity. This analyzer consists mainly of a low power Laser transmitter (0.5 W) and a receiver that may be conveniently separated by a distance of one meter as shown in Figure 2-b. Particles/or bubbles passing through the control volume of the two Laser beams intersection generate a fringe pattern in the surrounding space. The spatial frequency of this interference fringe pattern is inversely proportional to the particle size. In order to measure the spacing of this interference fringe pattern, three detectors were located at a selected spacing behind the receiver aperture. As the fringes move past the detectors at the Doppler difference frequency, they produce identical signals but with a phase shift. Signals from the detectors were amplified and transferred to the signal processor. The system was interfaced to an IBM PC/AT computer. The processed data were amplified and displayed on the oscilloscope screen and then plotted in histogram form on the data management computer's monitor. After data acquisition, a complete description for the particle size distribution, mass flux, density, mean and RMS velocity were obtained. Measurements using PDPA technique was found to be in good agreement (within ± 10% on the arithmetic and Sauter mean diameters [10] and within ±1% on the measured velocities [11]) with measurements obtained by other

techniques. Full details of the optical system, theory, calibration and operation of the analyzer are given in References 16 and 23.

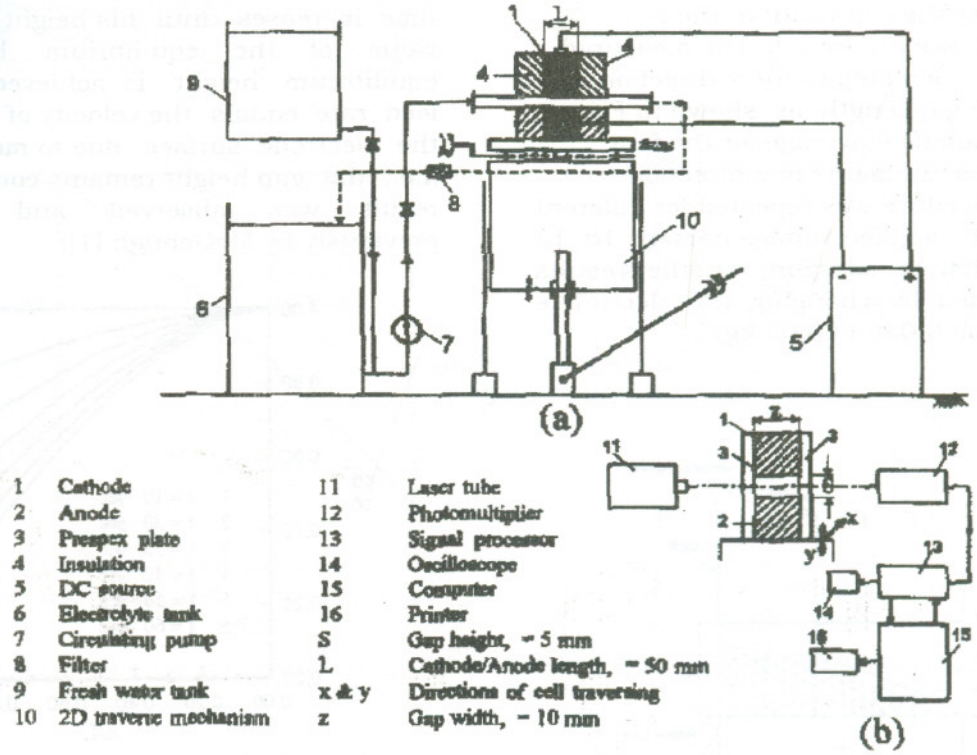

Figure 2 General layout of the experimental appartus. (a) Test rig layout; (b)Schematic diagram of the measurement technique.

In order to measure the bubbles layer thickness or the so called flow void fraction along the machining gap, the optical system was operated and the control volume of the intersection of the two Laser beams can be adjusted to lie at the mid of gap width (z), as seen in Figure 2-b. During ECM process, intensity of the transmitted Laser light will be decreased due to scattering and absorbing by the hydrogen bubbles. Thereon, noticing the amplified signals from the analyzer detectors on the oscilloscope screen when the cell moves upward or downward gives indication about the outer surface location of the bubbles layer. Moving the cell using the ability of vertical elevation on the 2D traverse system and observing the cell position which corresponds to the moment of signal variation on oscilloscope screen gives the bubbles layer thickness at this point of measurements.

Experimental procedure

The following procedure was carried out during the experimental program:

i. The electrolyte was pumped from the electrolyte tank through the cell across the inter-electrode gap. Then the DC current was connected to the cathode and the anode and consequently the bubbles layer appears within the gap.
ii. Aligning the optical system and checking the analyzer output.
iii. During each experiment, measurements were recorded over successive forward steps of 1 cm starting from the gap

entrance and along the gap length (i.e., in the x-direction), see Figure 3, and at a height of 1 mm from cathode surface. In each step, four radial measurements between each 2 mm have been carried out across the gap width in the z-direction, see Figure 2-b. The measured values at each step in the x-direction along the gap length, as shown in Figure 3, is a statistical average for the four radial measurements in z-direction.

This procedure was repeated for different values of the applied voltage namely; 10, 13 and 16 Volts. In addition, another results were obtained by changing the electrolyte flow rate from 0.036 to 0.05 kg/s.

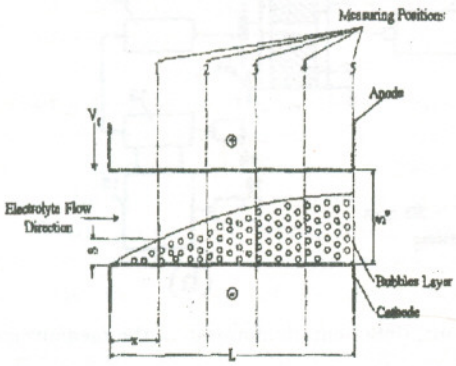

Figure 3 Flow behaviour and measuring stations along an ECM gap.

RESULTS AND DISCUSSION

Theoretical results presented in the following have been obtained using the computer program which was described in the preceding section to predict the characteristics of the bubbly two-phase flow during ECM processes in a rectangular gap similar to that shown diagramatically in Figure 1. Gap dimensions are for the cross-section and length as (5 mm × 10 mm) and 50 mm respectively. These dimensions are kept fixed in all the predictions obtained below. Figure 4 declares the plot of dimensionless gap height (S/S_i) versus dimensionless gap length (x/L) for different values of the machining time and at constant feeding velocity of 1.0 mm/min. Other boundary conditions are as follows; P_i = 2.0 bar, T_i = 300.0 K, E = 10.0 V and L = 0.05 m. It is seen that the gap height decreases continuously as the machining time increases until this height reaches the value of the equilibrium height. The equilibrium height is achieved when the feed rate equals the velocity of recession of the electrode surface due to metal removal (i.e., the gap height remains constant). This result was observed and discussed previously by McGeough [1].

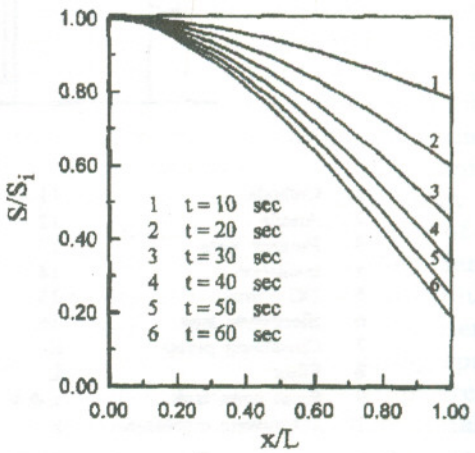

Figure 4 Variation of gap height with machining time at constant feeding velocity (1.0 mm/min).

The results illustrated in Figures 5 -7 show the effects of changing the applied voltage, electrolyte pressure and electrolyte temperature on the bubbly flow characteristics during ECM processes along the tested gap. In these figures, it will be noticed generally the pressure decreasing and increasing of electrolyte temperature rise, void fraction and mean bubble size along the gap length. Figure 5 reveals also that as the applied voltage (E) increases, the temperature rise (ΔT), void fraction (β) and the mean size (d) of the bubble are increased along the gap. This can be explained as, an increase of E leads to increase ΔT as the numerators of the right sides in Equations 9 and 13 are increased. This tendency causes (β) and (d) to be increased as shown in Equations 7 and 18. Variation of the two-phase flow characteristics along such a gap

with changing the electrolyte inlet pressure is illustrated in Figure 6. It can be seen here that, increasing electrolyte inlet pressure tends to increase the total pressure drop along the gap and then decreasing ΔT; β and d at the same time. This is because increasing electrolyte pressure compresses the bubbles layer and then causes the bubble size to be decreased. This conclusion was reported previously by McGeough [1] who showed that the bubble diameter appeared to be experimentally proportional to the (pressure)$^{-0.3}$.

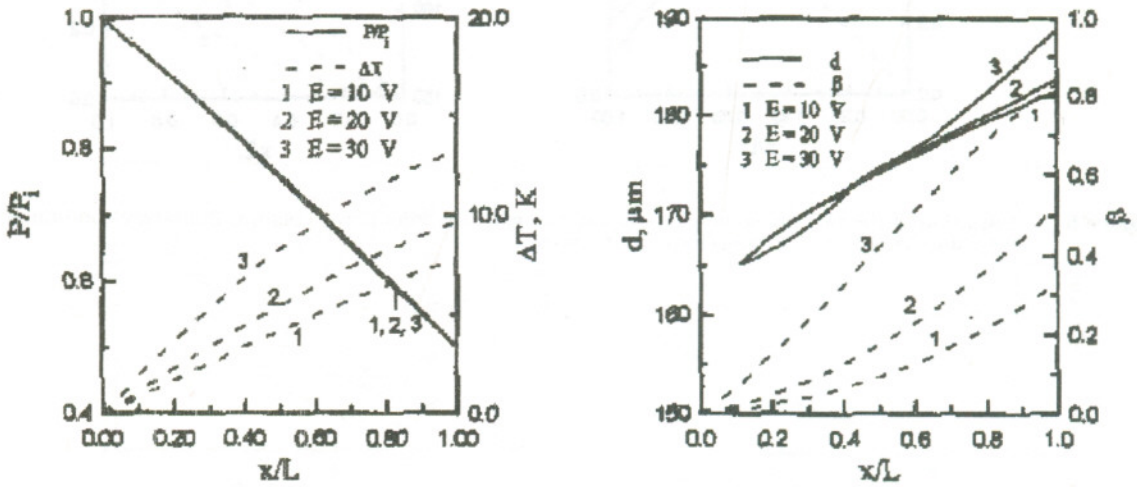

Figure 5 Variation of the two-phase flow characteristics with the applied voltage. Boundary conditions: P_i=2.0 bar, T_i=300 K, L=0.05m, V_f=1.0 mm/min and t = 30.0 s

The effect of electrolyte heating ahead the gap entrance on the two-phase flow characteristics is illustrated in Figure 7. In this figure, it is evident that heating the electrolyte before electrolysis did not affect the pressure drop through the cell whilst decreases slightly ΔT, β and d. Constancy of electrolyte pressure drop along the gap that showed in Figure 7 is understood with the aid of Equation 20. Attentiveness to the right side of this empirical equation indicates a feeble effect for the electrolyte temperature on the electrolyte properties that are used in calculating the predicted pressure drop. Slight decrease of ΔT, β and d for the bubbly flow along the gap with increasing the electrolyte initial temperature is explained also with the small changes that occur in the two-phase flow properties as the electolyte temperature increases. For example, Equation 25 shows that the bubble departure size is slightly affected by the electrolyte temperature variation through the small changes in both γ_e and γ_H.

Now, present model released limitations for the exit two-phase flow parameters at different operating conditions as presented in Figure 8. In this figure, it is apparent that the temperature rise, void fraction and mean size of bubbles at the gap exit are increased with increasing both the applied voltage and gap length within the ranges of (10 V< E < 50 V) for the applied voltage and (0.05 m < L < 0.2 m) for the investigated gap length.

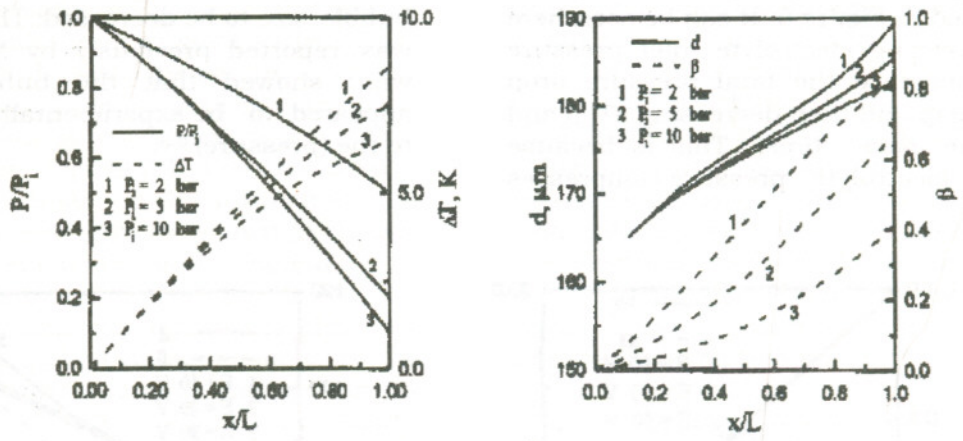

Figure 6 Variation of the two-phase flow characteristics with the inlet flow pressure. Boundary conditions: T_i =300K,L =0.05m, E=24 V, V_f=1.0 mm/min and t=60.0s.

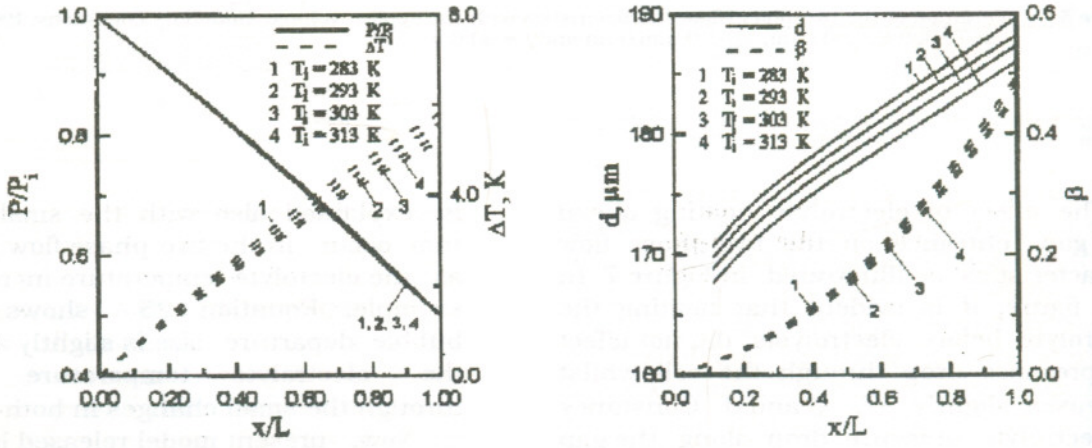

Figure 7 Variation of the two-phase flow characteristics with the inlet flow temperature. Boundary conditions: P_i =2.0 bar, L= 0.05.m , E = 13.0 V, V_f = 0.7 mm/min and t=60.0s.

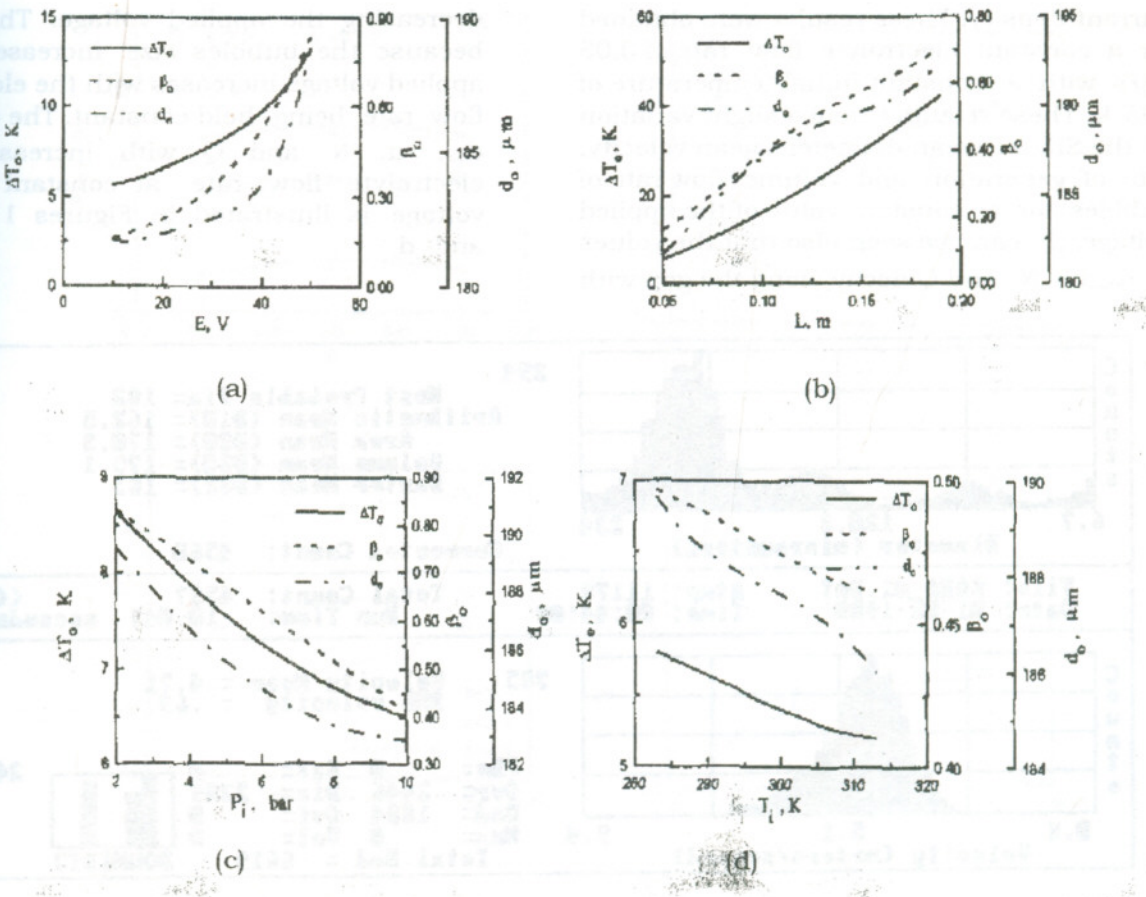

Figure 8 Limitations of exit two-phase flow parameters with: a-the applied voltage, b- the gap length, c- electrolyte pressure, and d- electrolyte temperature.

Furthermore; it can be seen also in Figure 8 that the parameters ΔT_o , β_o and d_o are decreased with increasing the initial values of flow pressure and electrolyte temperature within the investigated ranges of (2 bar < P_i < 10 bar) for flow pressure and (280 K < T_i < 320 K) for electrolyte temperature. Limitations which were illustrated in Figure 8 can serve in the correct selection of the operating parameters through an ECM process. The Appendix presents correlations for the variations of ΔT_o , β_o and d_o with the investigated operating parameters (i.e., E, L, P_i and T_i).

Phase distribution during flow of the electrolyte through the inter-electrode gap is given in Figure 3 for the case of system operation. This figure indicates the expected growth of the bubble layer as well as the gap dimensions. A typical set of distributions, which were obtained experimentally from the analyzer for the size and velocity of hydrogen bubbles in the gap is presented in Figure 9. These measurements are displayed in Figures 10 and 11 for different values of the applied voltage and electrolyte flow rate, respectively. The measured values in these figures are plotted against a dimensionless length equals the ratio of the distance between the measuring step and the gap entrance, x, to the gap length, L. Figures 10 -a,-b,-c and- d depict the variations of Sauter mean diameter (d_{32}), mean velocity (u), rate of bubbles generation $\dot{N}$ and volume flow rate (Q) for hydrogen bubbles along the gap with changing the applied voltage or

current density. These results were obtained for a constant electrolyte flow rate of 0.05 kg/s with a constant initial temperature of 295 K. These results reveal a slight variation of the Sauter mean diameter, mean velocity, rate of generation and volume flow rate of bubbles for a constant value of the applied voltage. It can be seen also that the values of d_{32},u, $\dot{N}$ and Q decay along the gap with decreasing the applied voltage. That occur because the bubbles size increases as the applied voltage increases with the electrolyte flow rate being held constant. The decay in d_{32}, u, $\dot{N}$ and Q with increasing the electrolyte flow rate at constant applied voltage is illustrated in Figures 11-a,-b,-c and- d.

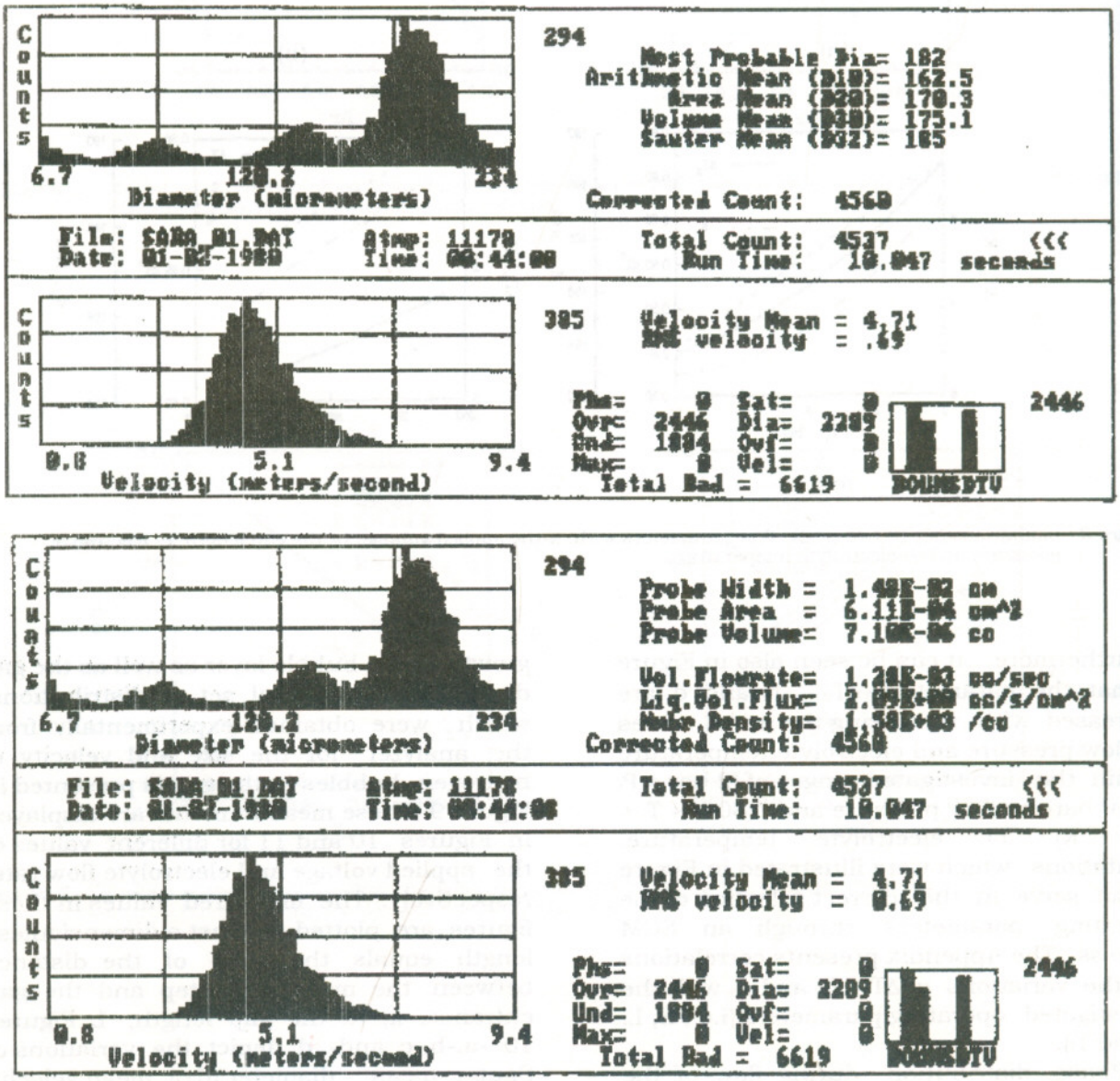

Figure 9 Typical distributions for the size and velocity of hydrogen bubbles in the ECM gap.

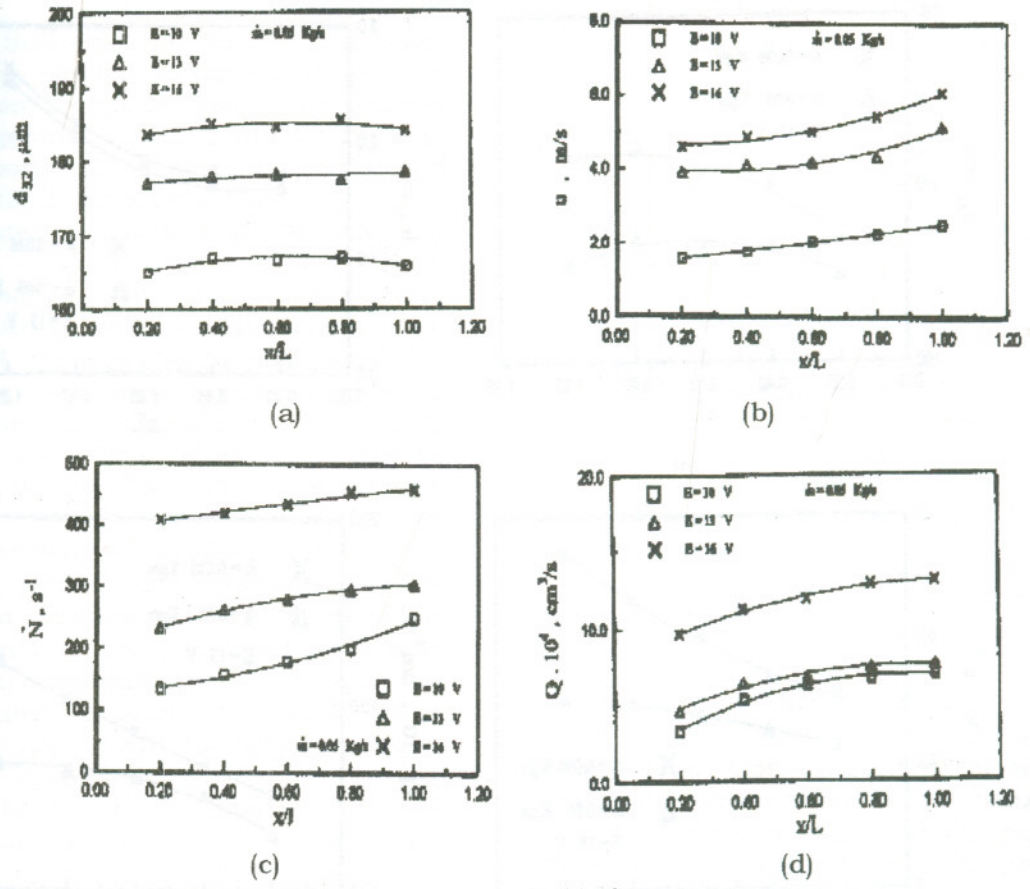

Figure 10 Effect of the applied voltage upon the size, velocity, rate of generation and volume flow rate of hydrogen bubbles through the investigated gep.

Here, it is interesting to note that, the bubbles velocity tends to increase along the gap for a constant electrolyte mass flow rate as shown in Figure 11-b. This is because the gas void fraction increases along the gap due to the accumulation of new bubbles at the cathode surface. Considering the principle of continuity, increasing the bubbles size or void fraction along the gap as clearly appears in Figure 11-a causes the velocities of electrolyte and hydrogen bubbles as well as the relative velocity between the two phases to increase [6] as depicted in Figure 11-b. Consequently, rate of generation and volume flow rate of bubbles phase will increase along the gap, see Figures(11-c and d). On the other hand; Figures (11-a,-b,-c and -d) reveal that increasing electrolyte flow rate yields a decrease in the Sauter mean diameter, rate of generation and volume flow rate of bubbles along the gap. The exact reason for this tendency is the diminishing of bubbles size with increasing the electrolyte flow rate.

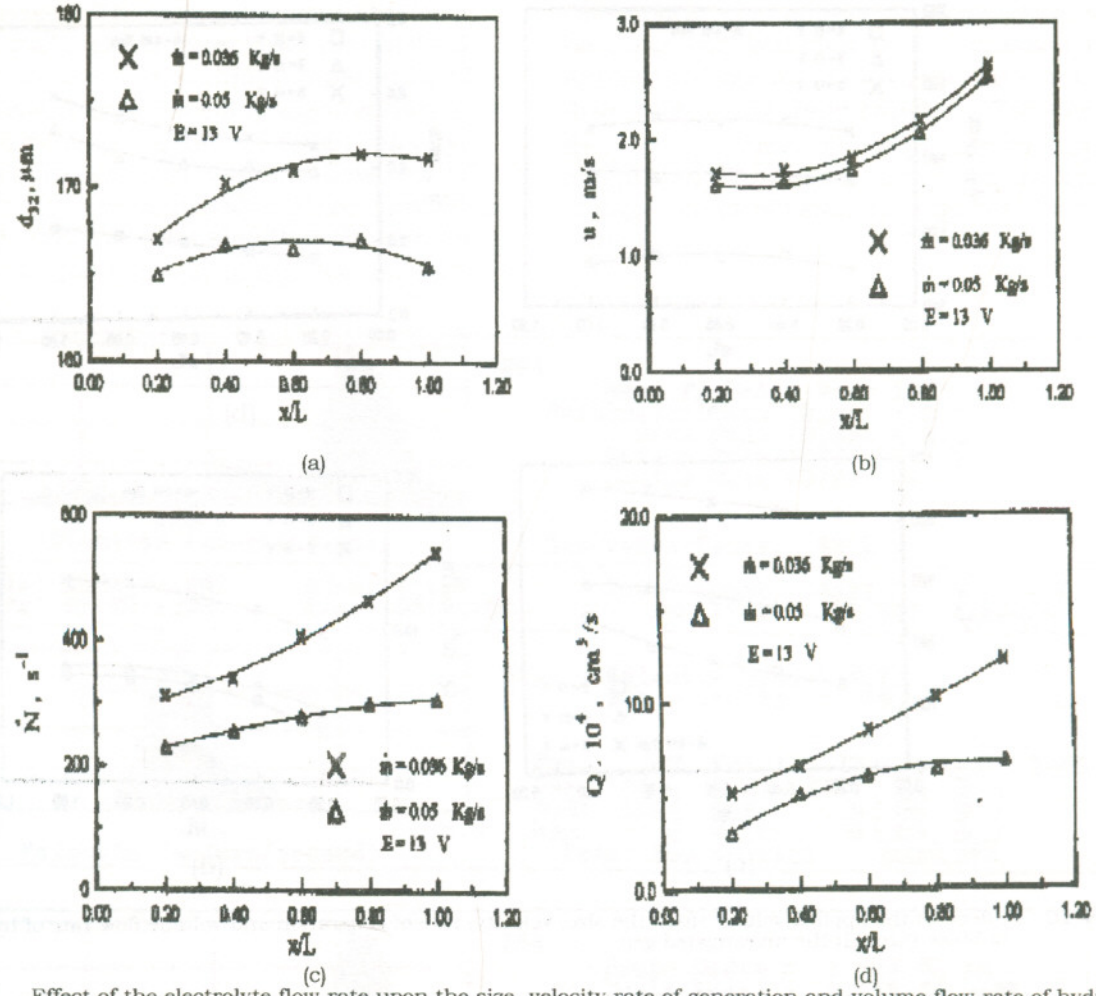

Figure 11 Effect of the electrolyte flow rate upon the size, velocity,rate of generation and volume flow rate of hydrogen bubbles through the investigated gap.

Figures 12 and 13 illustrate the influence of both the applied voltage and electrolyte flow rate on the variations of flow void fraction along the tested gap length. The void fraction is presented here as the bubble layer thickness at the measuring location divided by the gap height. This fraction is plotted in these figures against a dimensionless length. These figures show firstly that, the void fraction or the dimensionless thickness of bubbles layer increases in the downstream direction along the gap length. This increment of void fraction may be due to the accumulation of bubbles generated in locations along the gap. This tendency is observed and it is also reported by Landolt and others [13].

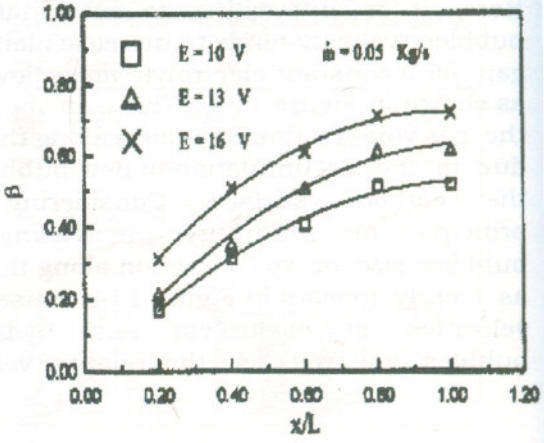

Figure 12 Influence of the applied voltage on flow void fraction along the length of the tested gap.

Figure 12 indicates that, for a constant flow rate as the applied voltage increases the void fraction increases also. This because the hydrogen bubbles diameter increases in direct proportional to current density and consequently the applied voltage [13]. Figure 13 illustrates the effect of changing the electrolyte mass flow rate, at a constant applied voltage, on the void fraction variation during cell operation. Here, it can be noticed that increasing the electrolyte flow rate or its velocity tends to decrease β or to decrease the thickness of bubbles layer along the gap. This tendency can be explained by the fact that the size of hydrogen bubbles decreases as the electrolyte velocity is increased [13].

Finally, predictions of bubbles size and void fracion variations along the tested gap are compared to the measured ones from present experimental program in Figure 14. The calculated variations of d and β are in good agreement with the measurements. The close agreement in Figure 14 can confirm both the theoretical and experimental results.

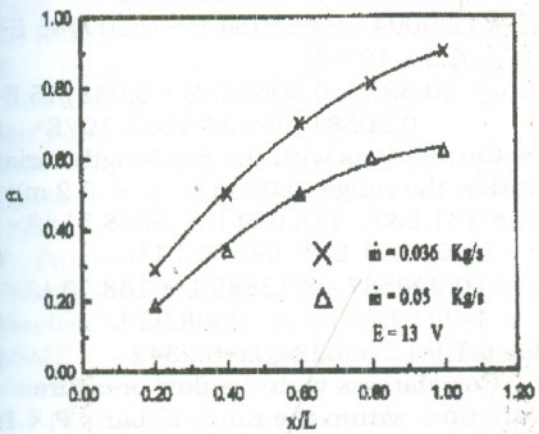

Figure 13 Influence of the electrolyte flow rate on the flow void fraction along the length of the tested gap.

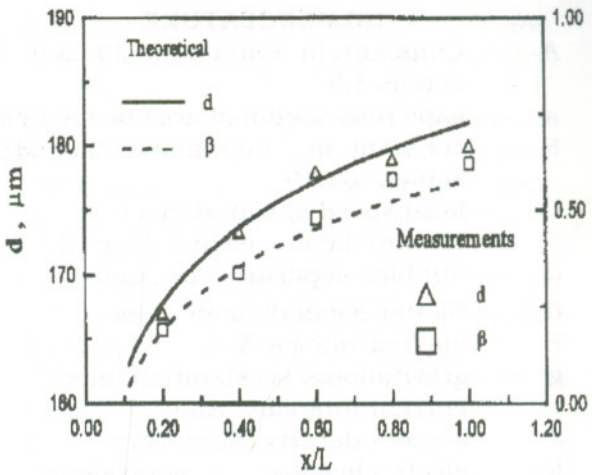

Figure 14 A comparison between predictions and measurements of both bubbles size and void fraction variations along the tested gep. Boundary conditions: E=13V, P_i=2.0 bar, T_i = 295 K, m=0.05 kg/s, V_f = 0.0mm/min and t =120.0s

CONCLUSIONS

The analytical and experimental results released in this paper appear to give a reasonable description for the behaviour of the two-phase bubbly flow characteristics through such a gap during ECM processes. The theoretical results indicate that decreasing both the value of initial flow pressure and electrolyte temperature as well as increasing the applied voltage tend to increase the flow void fraction, mean bubbles size and the two-phase flow temperature rise. However, predictions of the present suggested model show that changing flow pressure has the unique effect on the calculated pressure drop along an ECM gap. Moreover; these theoretical results declare the limits of void fraction, mean bubbles size and temperature rise that must be considered in an ECM process. Whilst analyzing the experimental results indicates that; the size, velocity, number and flow rate of bubbles together with the flow void fraction are increased with increasing the applied voltage and with decreasing the electrolyte flow rate.

NOMENCLATURE

A	Constant in Equations 20 and 24, equals 5.5
a	gap cross-sectional area (a = S.z), m^2
B	constant in Equations 20 and 24, equals -0.019
C	local speed of sound, ms^{-1}
C_p	isobaric heat capacity, $J.kg^{-1}.K^{-1}$
d_{oj}	bubbles departure size, mm
d_{32}	Sauter mean diameter, μm
E	applied voltage, V
g	gravitational acceleration, $m.s^{-2}$
I	current intensity, Amp
J	current density, Amp. cm^{-2}
K_H	electrochemical equivalent of hydrogen, gc^{-1}
K_M	electrochemical equivalent of the metal, gc^{-1}
L	gap length, mm
$\dot{m}$	electrolyte mass flow rate, $kg.s^{-1}$
N	number of bubbles in the mixture element
$\dot{N}$	rate of bubbles generation, s^{-1}
P	pressure, bar
Q	volume flow rate of hydrogen bubbles, $cm^3.s^{-1}$
R_H	gas constant of hydrogen, $J.Kg^{-1}.K^{-1}$
r	bubble radius, μm
S	gap height, mm
T	temperature, K
t	time, s
u	flow velocity, $m.s^{-1}$
V_f	feed rate, mm. min^{-1}
x	coordinate, distance along gap length, m
z	gap width, mm
α	wetness fraction
β	void fraction
γ	specific weight, $N.m^{-3}$
ε	temperature coefficient of conductivity, K^{-1}
η_H	current efficiency of hydrogen generation
η_M	current efficiency of metal removal
λ	thermal conductivity, $J.m^{-1}.hr^{-1}.K^{-1}$
μ	dynamic viscosity, $N.s.m^{-2}$
ν	kinematic viscosity, $m^2.s^{-1}$
ρ	density, $Kg.m^{-3}$

Subscripts

a	anode
e	electrolyte
g	gaseous phase
H	hydrogen
i	initial condition
l	liquid phase
M	metal
o	exit condition

Abbreviations

ECM	electrochemical machining
LDV	Laser Doppler Velocimeter
PDPA	Phase/Doppler Particle Analyzer
RMS	root mean square
2D	two dimensional

APPENDIX

In order to generalize the limitations which were presented in Figure 8 for the exit two-phase flow parameters, interpolated formulae for these parameters at different operating conditions have been carried out. These formulae are given below as functions of the investigated conditions and within certain ranges as;

a- Correlations with the applied voltage variation within the range (10 V < E < 50 V):

$$d_o = 203.48 - 2.19664\,E + 0.08873\,E^2 - 0.0016283\,E^3 + 1.11663\times10^{-5}E^4 \quad \text{(A-1)}$$

$$\beta_o = 1.30094 - 0.055954\,E + 0.309786\,E^2 - 6.3\times10^{-6}\,E^3 \quad \text{(A-2)}$$

$$\Delta T_o = 20.387 - 0.99652\,E + 0.033115\,E^2 - 0.305811\,E^3 + 3.99207\times10^{-7}E^4 \quad \text{(A-3)}$$

b- Correlations with the gap length variation within the range (0.05 m < L < 0.2 m):

$$d_o = 181.882 - 175.024\,L + 5038.51\,L^2 - 36202.1\,L^3 + 84578.1\,L^4 \quad \text{(A-4)}$$

$$\beta_o = 0.228587 - 8.13689\,L + 188.73\,L^2 - 1152.79\,L^3 + 2388.92\,L^4 \quad \text{(A.5)}$$

$$\log(\Delta T_o) = 1.50303\log(L) + 6.2342 \quad \text{(A-6)}$$

c- Correlations with the flow pressure variation within the range (2 bar < P_i < 10 bar):

$$d_o = 193.178 - 2.01048\,P_i + 0.098165\,P_i^2 \quad \text{(A-7)}$$

$$\beta_o = 0.943458 - 0.0553374\,P_i + 0.00022916\,P_i^2 \quad \text{(A-8)}$$

$$\Delta T_o = 9.60183 - 0.51052P_i + 0.02021266P_i^2 \quad \text{(A-9)}$$

d- Correlations with the electrolyte temperature variation within the range (280 K <T_i < 320 K):

$$d_o = 5576.09 - 53.9964\ T_i + 0.180616\ T_i^2 + 0.000201668\ T_i^3 \quad \text{(A-10)}$$

$$\beta_o = -30.007 + 0.312595\ T_i - 0.0010633\ T_i^2 + 1.2 \times 10^{-6}\ T_i^3 \quad \text{(A-11)}$$

$$\Delta T_o = -375.164 + 3.94676\ T_i - 0.0135524 T_i^2 + 1.54168 \times 10^{-5} T_i^3 \quad \text{(A-12)}$$

d_o and ΔT_o are released from the above equations in μm and K respectively.

REFERENCES

1. J.A. McGeough, "Principles of Electrochemical Machining", Chapman and Hall, London, (1974).
2. V.K. Jain, Vinod Kumar Jain and P.C. Pandey, "Corner Reproduction Accuracy in Electro-Chemical Drilling (ECD) of Blind Holes", Trans. ASME, J. of Engineering for Industry, Vol. 106, pp. 55, (1984).
3. C.N. Larsson, "Fine Hole Drilling in a Titanium Alloy Using ECM", Proc. 2nd Joint Symposium on Manufacturing Engg., England, pp. 167, (1979).
4. D.V. Krishnaiah Chetty, R.V.G.K Murthy, and V. Radhakrishnan, "On Some Aspects of Surface Formation in ECM", Trans. ASME, J. of Engineering for Industry, Vol. 103, pp. 341, (1981).
5. E. Rumyantsev, and A. Davydov, "Electrochemical Machining of Metals", Mir Publishers, Moscow, (1989).
6. G.B. Wallis, "One-dimensional Two-Phase Flow", McGraw-Hill, New York, (1969).
7. F. Fluerenbrock, R.D. Zerkle, and J.F. Thorpe, "Compressibility Effects in Electrochemical Machining", Trans. ASME , J. of Engineering for Industry, Vol. 98, pp. 423, (1976).
8. A.F. Stronach, J.A. McGeough and W.G. Clark, "Experimental and Numerical Analysis of the Pressure Distribution in Electrochemical Machining", Int. J. Mechanical Science, Vol. 18, pp. 261, (1976).
9. S.P. Loutrel and N.H. Cook, "A Theoretical Model for High Rate Electrochemical Machining", Trans. ASME, J. of Engineering for Industry, Vol. 95, pp. 1003, (1973).
10. A.M. Abdel Mahboud , "Workpiece Shape Errors in Electrochemical Machining", Port-Said Faculty of Engng. Scientific Engineering Bulletin , Vol. 5, pp. 251, (1993).
11. I. Rousar, K. Micka, and A. Kimla, "Electrochemical Engineering", Part 2, Academia Publ., Praha, (1986).
12. B.J. Azzopardi, "Measurements of Drop Sizes", Int. J. Heat Mass Transfer, Vol. 22, pp. 1245, (1979).
13. D. Landolt, R. Acosta, R.H. Muller, and C.W. Tobias, "An Optical Study of Cathodic Hydrogen Evolution in High Rate Electrolysis", J. of Electrochemical Soc., Vol. 117(6), pp. 839, (1970).
14. C.Y. Yu, Z.Y. Hou, X.K. Yao, and Y.S. Yang, "The Experimental Investigation on Gas Bubble Distribution in Electrochemical Machining Gap", 7th International Symposium on Electro-Machining (ISEM 7), UK, pp. 393, (1983).
15. O.V. Krishnaiah Chetty, and V. Radhakrishnan, "Electrolyte Velocity Measurement Using LDV in an Experimental Electrochemical Machining Setup", Int. J. of Machine Tool Design Res., Vol. 9 (3), pp. 157, (1979).
16. M.J. Houser, and W.D. Bachalo, "Extension of the Phase/Doppler Particle Analyzer to Submicrone Particle Measurements", Proc. of SPIE-The International Society for Optical Engineering, 573, pp. 57, (1985).
17. T.I., Sabry, A.M. Abdel Mahboud, and N.H. Mahmoud, "Experimental Investigations Into Two-Phase Bubbly Flow in an Electrochemical Machining Gap", 4 th Int. Conf. of Fluid Mechanics (ICFM4), Alexandria Univ., Alexandria, Vol. IV, pp. 203, (1992).
18. K. Lubkowski, J. Kozak, L. Dabrowski, and A.M. Abdel Mahboud, "Some Problems of Optimization of Electrochemical Machining (ECM)", 4 th Int. Conf. of Mechanical Design and

Production, Cairo Univ., Cairo, pp. 535, (1988).
19. J.G. Collier, "Convective Boiling and Condensation", Chapter 4, McGraw-Hill, New-York, (1981).
20. A.E. Bergles, J.G. Collier, J.M., Delhaye, G.F. Hewitt and F. Mayinger, "Two-Phase Flow and Heat Transfer in the Power and Process Industries", McGraw-Hill, New-York, (1981).
21. ASHRAE, Guide and Data Book, American Soc. of Heating; Refrig; and Air-Cond. Engineers, New-York, (1965).
22. R.H. Perry, and C.H. Chilton, (Eds), "Chemical Engineers Handbook", 5th Edition, McGraw-Hill, Tokyo, (1973).
23. W.D. Bachalo, R.C. Rudoff, and M.J. Houser, "Laser Velocimetry in Turbulent Flow Fields: Particle Response", AIAA 25 th Aerospace Sciences Meeting, Reno, Nevada, USA, pp. 1, (1987).

Received March 19,1998
Accepted June 15, 1998

بحوث نظرية وتجريبية فى السريان ثنائى الطور الفقاعى خلال فتحة تشغيل الكتروكيميائى

طاهر إبراهيم صبرى* ، نبيل حنفى محمود* و عادل محمود عبد المعبود**

* قسم هندسة القوى الميكانيكية – جامعة المنوفيه

** قسم هندسة الانتاج والتصميم الميكانيكى – جامعة المنوفية

ملخص البحث

تطرح هذه الورقة نموذجا نظريا للتنبؤ بتوزيعات الضغط – ارتفاع درجة الحرارة – القطر المتوسط للفقاعات وجزء الفراغ (الغاز) خلال سريان فقاعى ثنائى الطور فى فتحة تشغيل الكتروكيميائى ، ولقد أسس هذا النموذج على معادلات بقاء الكتلة والطاقة لسريان فقاعى أحادى البعد وغير مستقر ، يهتم البرنامج المعملى فى هذا العمل باستخدام تقنية محلل الجسيمات من نوع الطور / دوبلر وذلك فى قياسات السريان ثنائى الطور خلال طبقة غاز الايدروجين على طول الفتحة ، وهنا فإن التجارب تقدم أنماط توزيعات السرعة – الحجم – معدل تولد وتدفق فقاعات الايدروجين ، كما تقدم التجارب أيضا أنماط توزيع سمك طبقة الفقاعات على طول فتحة التشغيل الالكتروكيميائى المختبرة عند قيم مختلفة لجهد التيار المستمر ومعدل تدفق الالكتروليت(المائع المتحلل بالكهرباء).

تظهر النتائج النظرية أن الخصائص المميزة لسريان ثنائى الطور فقاعى عبر فتحة تشغيل الكتروكيميائى مختبره تتأثر بجهد التيار المستمر – طول الفتحة – ضغط الالكتروليت ودرجة حرارته ، تم التأكيد على مقارنة قياسات محلل الجسيمات من نوع الطور / دوبلر لكل من قطر الفقاعات المتوسط وجزء فراغ السريان مع التنبؤات المأخوذة من النموذج النظرى ، ولقد أعطت المقارنه توافقا جيدا وتاما بين القياسات المعملية والتنبؤات النظرية للنموذج الحالى ، كذلك فقد أظهرت هذه المقارنة أن التقريب أحادى البعد للسريان يعد كافيا عند إجراء الحسابات للسريان الفقاعى ثنائى الطور خلال فتحة تشغيل الكتروكيميائى ذات مقطع قائم الزوايا (مربع أو مستطيل).